EXPLORING THE NONLINEAR DYNAMICS OF IRIS DEFORMATION

ANTWAN D. CLARK

Computational Medicine Imaging and Modeling Center, Rutgers University, 617 Bowser Road Piscataway, New Jersey 08854, United States of America

aclark.biometrics@gmail.com

SCOTT A. KULP

Computational Medicine Imaging and Modeling Center, Rutgers University, 617 Bowser Road Piscataway, New Jersey 08854, United States of America

sckulp@cs.rutgers.edu

ISOM H. HERRON

Department of Mathematical Sciences, Rensselaer Polytechnic Institute, 110 8th Street Troy, New York 12180, United States of America

herroi@rpi.edu

ARUN A. ROSS

Lane Department of Computer Science and Electrical Engineering, West Virginia University, P.O. Box 6070 Evansdale Drive Morgantown, West Virginia 26506, United States of America

arun.ross@mail.wvu.edu

We present a novel approach using what we know about biomechanics to explore the nonlinear dynamics of iris deformation. Current iris recognition systems and algorithms at most assume that the dilation is linear. Furthermore, research on iris deformation do not take into account the mechanical properties of the iris tissue as well as the cause of deformation, which is from the iris musculature. In our work, we explore the tissue mechanics of the iris region. From looking at the mechanics, we are able to get a complete understanding of the dynamics as well as disprove the current linear assumption.

Keywords: mathematical model; iris deformation; pupil dilation.

1. Introduction

Biometrics is the science of establishing human identity based on the physical or behavioral attributes of an individual such as fingerprints, face, iris, voice, gait and signature [8]. The deployment of biometric systems in several identity management and access control systems ranging from laptops to border security has demonstrated the potential of using biometrics for human recognition. Iris recognition systems, in particular, are gaining interest because the iriss rich texture offers a strong biometric cue for recognizing individuals [19]. Located just behind the cornea

and in front of the lens, the iris uses the dilator and sphincter muscles that govern pupil size to control the amount of light that enters the eye. Near-infrared (NIR) images of the iriss anterior surface exhibit complex patterns that computer systems can use to recognize individuals. Because NIR lighting can penetrate the iriss surface, it can reveal the intricate texture details that are present even in dark-colored irides. The iriss textural complexity and its variation across eyes have led scientists to postulate that the iris is unique across individuals. Further, the iris is the only internal organ readily visible from the outside. Thus, unlike fingerprints or palm prints, environmental effects cannot easily alter its pattern.

The history of iris recognition dates as early as 1936, yet was revolutionized in the mid 1990's when John Daugman [2] developed an algorithm to automate the identification of the human iris. Most iris recognition systems consist of five basic modules leading to a decision [19]:

- The *acquisition* module obtains a 2D image of the eye using a monochromatic CCD camera sensitive to the NIR light spectrum.
- The *segmentation* module localizes the iriss spatial extent in the eye image by isolating it from other structures in its vicinity, such as the sclera, pupil, eyelids, and eyelashes.
- The *normalization* module invokes a geometric normalization scheme to transform the segmented iris image from cartesian coordinates to polar coordinates.
- The *encoding* module uses a feature-extraction routine to produce a binary code.
- The *matching* module determines how closely the produced code matches the encoded features stored in the database.

The role of the normalization module is to convert the localized iris from a near-circular entity to a rectangular entity. The process, often called iris unwrapping, has three advantages:

- It accounts for variations in pupil size due to changes in external illumination that might influence iris size.
- It ensures that the irides of different individuals are mapped onto a common image domain in spite of the variations in pupil size across subjects.
- It enables iris registration during the matching stage through a simple translation operation that can account for in-plane eye and head rotations.

Daugman's algorithm incorporates a rubber-sheet model in order to normalize the effects of the pupil dilation to project the iris region to a fixed rectangle via $I(x(r,\theta), y(r,\theta)) \longmapsto I(r,\theta)$ given by the following transformation:

$$x(r,\theta) = (1-r)x_p(\theta) + rx_l(\theta) \qquad (1.1)$$
$$y(r,\theta) = (1-r)y_p(\theta) + ry_l(\theta)$$

where (x_p, y_p) and (x_l, y_l) correspond to the Cartesian coordinates of the pupil and limbus boundary respectively. After applying 1.1 to normalize the dilation effects, Daugman's algorithm uses Gabor wavelets in order to convert the instinctive information of the iris texture to a bit sequence used for comparison. Current commercial systems use Daugman's algorithms, which have shown to be fairly accurate and give really good performance. However, there still exist challenges in iris recognition, which would include looking at the case of varying levels of pupil dilation. Recently it was shown that varying degrees of pupil dilation have shown to degrade iris recognition performance. Hence, there is a need to explore ways to counteract pupil dilation and consequently iris deformation.

1.1. *Related work*

The problem of pupil dilation and iris deformation has recently been explored and noted by previous researchers in biometrics as well as other areas. In their work, Ma et. al [12] noticed that there were a number of false non-matches due to pupil dilation. Later, Thornton et. al [21] took pupil dilation into account with their work by using Bayesian estimation to recover the level of iris deformation. From taking the Bayesian estimation into account, their results illustrated that estimating the level of iris deformation leads to an improvement in iris recognition performance. In addition, Wei et. al [23] attempted to consider the effects of pupil dilation by modeling the nonlinear iris stretch as a sum of the linear stretch and Gaussian deviation term. Hollingsworth et. al [7] investigated this problem further via conducting experiments in order to extend the previous claims that it is the varying degrees of dilation that affect iris recognition performance.

Pupil dilation has been explored in other fields to include mathematical biology and more recently in computer graphics. Previous research have shown that in addition to changes in light intensity pupil motion is also dictated by levels of consciousness; focal length; heart rate; respiration; emotional factors; disease; and drug use. However, physiological models were created with taking variations of illumination into account because there is more supporting data based on this fact. Modeling the pupil dynamics began with performing empirical studies with varying light intensity and using the results to come up with a model. One of the famous models would be Moon and Spencer [13] where the following model was proposed based on experimental data:

$$D = 4.9 - 3\tanh(0.4(\log_{10}(L_b - 0.5)) \qquad (1.2)$$

where D us the pupil diameter (expressed in mm) and L_b is the background luminance (expressed in $Blondels$). There have been other models, but from the literature the Moon and Spencer model appears to be the most cited when it comes to estimating the average pupil size. Later it was realized that it is inherent to explore the pupil dynamics in order to understand the changes in pupil size given the varying degrees of illumination. Therefore, more experimental studies have been extended to explore this effect instead of simply relying on changes in pupil size. Ellis[3] performed experiments to determine the average latency as well as the maximum constriction and dilation velocities for a given light intensity. In turn, he found that the latency τ (expressed in ms) is described as:

$$\tau(L_{cd}) = 445.7 - 22.9L_{cd} + \ 76.2L_{cd}^2 \tag{1.3}$$

and the constriction V_c and dilation V_d velocities (expressed in mm/s) are described as:

$$V_c(L_{cd}) = 0.15 + \ 2.0L_{cd} - 0.17L_{cd}^2 \tag{1.4}$$

and

$$V_d(L_{cd}) = 0.16 + \ 0.72L_{cd} - 0.07L_{cd}^2 \tag{1.5}$$

In equations 1.3, 1.4, and 1.5 the variable L_{cd} represents the intensity of the light measured in $candelas/m^2$. Furthermore Link and Stark [10] empirically determined the pupillary latency, the time delay between that in which a light pulse reaches the retina and the beginning of the pupillary reaction which yields the following equation:

$$\tau(R, L_{fL}) = 253 - 14\ln(L_{fL}) + \ 70R - 29R\ln(L_{fL}) \tag{1.6}$$

where τ is the latency in ms, L_{fL} is the luminance in $foot - Lambert$, and R is the frequency in Hz.

From the empirical models came the physiologically-based models where the models were derived based on the physiological and anatomical observations without the reliance on experimental data. Usui and Stark [22] developed a parametric model of the iris to describe the pupil characteristics in response to light while using probability distribution functions to describe the random fluctuations. Later, Stark [20] concluded that the pupillary response can be viewed as a negative feedback dynamical system. Though this expression of the pupil dynamics is attractive, it was Longtin et. al [11] that was the first to express the dynamics of the pupil light reflex as a nonlinear delay differential equation given by

$$\frac{dg}{dA}\frac{dA}{dt} + \alpha g(A) = \gamma \ln\left[\frac{\phi(t-\tau)}{\overline{\phi}}\right] \tag{1.7}$$

where A is the pupil area; ϕ is the retinal light flux; and $\overline{\phi}$ is the light level there there is no pupillary response. Furthermore, τ is the time delay due to retinal processing, which includes responses from the midbrain nuclei; and $\gamma > 0$ is an arbitrary constant. In the derivation of equation 1.7, the pupil area is related to the activity of the iris muscle given by

$$A = f(x)$$

where $f(x)$ represents the activity of the iris muscle. Longtin defines this activity in terms of the Hill function given by

$$f(x) = \frac{\beta_1 \theta^n}{\theta^n + x^n} + \beta_2$$

where β_1 is the minimum pupil area; $\beta_1 + \beta_2$ is the maximum pupil area; and θ and n are positive constants. In his work, Longtin chose the Hill function because it best represents the fact that the pupil area is positive and has finite limits as well as it resembles the elastic properties of the iris muscle. The function $g(A)$ is the inverse of $f(x)$. In computer graphics, Pamplona [15] recently looked at Longtin's equation of the pupil light reflex in order to simulate the varying degrees of pupil dilation as well as iridal pattern deformation in animated human characters in order to enhance facial animation. In his work, Pamplona notes that though Longtin's model is well cited there are ambiguities with estimating the various parameters $(\alpha, \beta_1, \beta_2, \gamma, \theta, n, \overline{\phi})$. The selection of these parameters are important to ensure convergence as well as make sure that the simulations are as realistic as possible. By using the steady-state formulation of equation 1.7; making the comparison with the Moon and Spencer model; as well as making the appropriate conversions to the dynamic case yields

$$\frac{dM}{dD}\frac{dD}{dt} + 2.3026M(D) = 0.45 \ln\left[\frac{\phi(t-\tau)}{\overline{\phi}}\right] \tag{1.8}$$

where D is the pupil diameter and the function $M(D) = \tanh^{-1}\left(\frac{D-4.9}{3}\right)$.

Although the idea of pupil dynamics has been studied in different communities outside of biometrics, it does not appear to have much research on modeling iridal dynamics. It appears that Rohen [18] is the first researcher to study the collagen form of the iris. In his work, he proposed model for the collagen fibers assuming

that they are arranged in a series of parallel arcs, connecting the iris root to the pupil border in both clockwise and counter clockwise fashions. Later, Wyatt [24] used Rohen's formulation and created a mathematical formulation for iris deformation as a sum of a linear stretch and nonlinear deviation in order to demonstrate the wear and tear of the collagen fibers in the iris region. Wei et. al [23] used pattern recognition approaches and concluded that the nonlinear deviation is Gaussian. Finally, Pamplona used an imaged-based model for iridal deformation via tracking points on the pupil border as well as various feature points throughout the iris region. From there, he calculated the distance from the pupil center; the distance from the pupil border; and the percentage in the iris region with respect to the pupil diameter. With these results, he concluded that approximating the iridal deformation to be linear is good enough to give a realistic simulation.

1.2. *Our approach and motivation*

One of our main motivations for this work comes from Hollingsworth et. al. Their results show that there is a need to explore correcting the various degrees of pupil dilation in order to improve iris recognition. Our other motivation comes from the fact in our literature search on iris deformation there is a need to build a mathematical model to explore the physiological dynamics of the iris while considering the varying degrees of pupil dilation. Though the previous work (Thornton and Wei) took dilation into account in their corrections, they did not consider the varying degrees of pupil dilation. Furthermore, both Thornton and Wei used pattern recognition approaches, which are limiting because they are dependent on a particular dataset and are not necessarily based on the physiology of the iris. We also found Pamplona's image-based model to describe iridal deformation to not be fully complete because though the feature points might seemingly move in a linear fashion, it doesn't necessarily mean that the deformation is mostly linear. Having a realistic simulation might prove beneficial in computer graphics; however, the desire in biometrics and other biologically related fields is to be physically accurate as possible. Finally, Wyatt is also aware that his mathematical model is limiting because he stresses that his work is only a "meshwork skeleton" and does not form the basis for both linear and nonlinear iridal stretch, which comes from the variations in the elastic properties of the iris as well as the iris musculature. Thus, the work of Wei et. al is also limiting in this regard since they apply the "meshwork skeleton" to determine that the nonlinear stretch is Gaussian.

Here we present a novel approach to mathematically model iris deformation via the using what we know about biomechanics – the application of continuum mechanics to biological medium. With biomechanics, we can predict the nonlinear dynamics of the iris while considering the varying degrees of dilation. Doing so removes the reliance of pattern recognition as well as incorporates the elastic properties of the iris in addition to the muscle activity. After formulating our model, we will perform

mathematical analysis on our model within the confines of the annular region of the iris. Our mathematical analysis is done in two parts: we first look at the entire orthotropic case. Next, we consider the assumption that the iris region is isotropic. Though we adopt the assumption by Lei et. al [9] that the iris region is orthotropic, exploring the isotropic case could prove beneficial because we don't have the dependency of the material properties and could some insight into the orthotropic case formulation.

2. Mathematical Formulation

We begin our mathematical formulation by viewing the iris region as a thin cylindrical shell, where the thickness in the z dimension is much smaller compared to that of the r and θ directions. Hence, we can look at the region in terms of a thin plate where the loads are applied uniformly over the z dimension. With this thin plate formulation, we can also make the assumption that the normal stress in the z direction σ_z as well as the shear stresses τ_{rz} and $\tau_{\theta z}$ are negligible. This simplification reduces the dynamics of the iris region to the two-dimensional r-θ plane. Another observation is that the iris muscles (both the sphincter and dilator muscles) are equally distributed throughout the annular region. Therefore, we can also assume that the region and load are axisymmetric. Therefore mathematically we can also make the assumptions that $\frac{\partial}{\partial\theta}$ and u_θ are negligible, which consequently follows that the shear stress $\tau_{r\theta}$ is also negligible. With these assumptions, the stress and strain vectors become $\overrightarrow{\sigma} = \langle\sigma_r, \sigma_\theta\rangle$ and $\overrightarrow{\epsilon} = \langle\epsilon_r, \epsilon_\theta\rangle$ respectively with the following relationship:

$$\begin{aligned} \epsilon_r &= \frac{\sigma_r}{E_r} - \frac{\nu_{r\theta}}{E_\theta}\sigma_\theta \\ \epsilon_\theta &= -\frac{\nu_{\theta r}}{E_r}\sigma_r + \frac{\sigma_\theta}{E_\theta} \end{aligned} \tag{2.1}$$

where E_r and E_θ are the Young's moduli (i.e. the material properties of the iris region); $\nu_{r\theta}$ is the Poisson's ratio in the azmuthal direction; and $\nu_{\theta r}$ is the Poisson's ratio in the radial direction. It needs to be noted that for orthotropic formulation $\nu_{r\theta} \neq \nu_{\theta r}$; however, due to the symmetry with the stress and strain tensors, the following relationship must hold:

$$\frac{\nu_{\theta r}}{E_r} = \frac{\nu_{r\theta}}{E_\theta}. \tag{2.2}$$

Since the Poisson's ratio $\nu_{\theta r}$ (from Lei et. al. [9]) is known, we use the relationship given from 2.2 to simplify equation 2.1 to be:

$$\epsilon_r = \frac{\sigma_r}{E_r} - \frac{\nu_{\theta r}}{E_r}\sigma_\theta \qquad (2.3)$$
$$\epsilon_\theta = -\frac{\nu_{\theta r}}{E_r}\sigma_r + \frac{\sigma_\theta}{E_\theta}.$$

Solving for the stress terms σ_r and σ_θ achieves

$$\sigma_r = \frac{E_r}{(1-\zeta\nu^2)}(\epsilon_r + \zeta\nu\epsilon_\theta) \qquad (2.4)$$
$$\sigma_\theta = \frac{E_\theta}{(1-\zeta\nu^2)}(\nu\epsilon_r + \epsilon_\theta)$$

where $\nu = \nu_{\theta r}$ and $\zeta = \frac{E_\theta}{E_r}$. We next consider the fact that soft biological tissues, like the iris, experience finite (or large) strain. This affects the Cauchy relationships because the relationship between the strain components ϵ_r and ϵ_θ and the displacement u are completely nonlinear. Adopting our assumptions for the Cauchy equations reduces the components of the strain vector $\overrightarrow{\epsilon}$ to

$$\epsilon_r = u' - \frac{1}{2}(u')^2 \qquad (2.5)$$
$$\epsilon_\theta = \frac{u}{r} - \frac{1}{2}\left(\frac{u}{r}\right)^2$$

and the equilibrium condition reduces to

$$\frac{d\sigma_r}{dr} + \frac{\sigma_r - \sigma_\theta}{r} = 0\ . \qquad (2.6)$$

In equation 2.5, we drop the subscripts because our problem now simplifies to only examining variations in the radial displacement u_r. We also use the primes $()'$ to denote ordinary differentiation with respect to r because the displacement only depends on the radial component (i.e. $u = u(r)$). Substituting equation 2.5 into equations 2.1 and 2.6 yields the following differential equation:

$$u'' + \frac{u'}{r} - \frac{\zeta u}{r^2} - \frac{(1-\nu\zeta)}{2r}(u')^2 - \frac{(\nu-1)\zeta}{2r}\left(\frac{u}{r}\right)^2 - \frac{1}{2}\frac{d}{dr}(u')^2 - \frac{\nu\zeta}{2}\frac{d}{dr}\left(\frac{u}{r}\right)^2 = 0 \qquad (2.7)$$

where ζ is given by

$$\zeta = \frac{E_\theta}{E_r} \tag{2.8}$$

and E_r and E_θ are the radial and azimuthal Young's moduli respectively. The boundary conditions in equation 2.7 on the annular domain $r \in (r_1, r_2)$ are

$$u(r_1) \ = \mu_1, \ \mu_1 > 0 \tag{2.9}$$

and

$$u(r_2) = 0. \tag{2.10}$$

Examining equation 2.7 shows that iris deformation is nonlinear. However, we will like to theoretically analyze the behavior of the displacement $u(r)$ inside of the annular region $r \in (r_1, r_2)$. This will be done by analyzing 2.7 given the boundary conditions 2.9 and 2.10. Performing the mathematical analysis provides the overall complete picture of the iridal dynamics.

2.1. *Mathematical analysis – orthotropic deformation*

The mathematical analysis is done by taking advantage of the following theorem to show uniqueness[16]:

Theorem 2.1. *Let $u(r)$ be a solution of the boundary value problem*

$$u'' + H(r, u, u') = 0 \text{ for } r_1 < r < r_2, \tag{2.11}$$

$$\left.\begin{array}{l} u(r_1) = \gamma_1, \\ u(r_2) = \gamma_2. \end{array}\right\} \tag{2.12}$$

Suppose that $H, \partial H/\partial u$, $\partial H/\partial u'$ are continuous and that $\partial H/\partial u \leq 0$. Then a solution to (2.11) which also satisfies (2.12) is unique.

In order to take advantage of theorem 2.1 we expand equation 2.7 to get the following:

$$(1-u')u'' + \frac{u'}{r} - \frac{\zeta u}{r^2} - \frac{(1-\nu\zeta)}{2r}(u')^2 - \frac{(\nu-1)\zeta}{2r}\left(\frac{u}{r}\right)^2 - \nu\zeta\left(\frac{uu'}{r^2} - \frac{u^2}{r^3}\right) = 0. \tag{2.13}$$

In order to get the form that we desire we replace u by $-u$ and arranging to get the following form as in 2.11 where

$$H = -\frac{1}{(1+u')}\left[-\frac{1}{r}u' + \frac{\zeta}{r^2}u + \frac{\nu\zeta - 1}{2r}(u')^2 + \frac{(1-\nu)\zeta}{2r^3}u^2 - \nu\zeta\left(\frac{u'u}{r^2} - \frac{u^2}{r^3}\right)\right]. \tag{2.14}$$

with the boundary conditions given from 2.9 and 2.10. Looking at the annular domain of the iris region $r \in (r_1, r_2)$ we see that the length of the domain is fairly small and hence it is safe to make the assumption that the solution u behaves in the manner such that$|u'(r)| < 1$. Furthermore, since the rest of the expression inside the brackets of the expression in 2.14 is in polynomial form then it is safe to conclude that H and its derivatives are continuous.

Next, we compute $\partial H/\partial u$ and get the following expression:

$$\frac{\partial H}{\partial u} = -\frac{1}{(1+u')}\left[\frac{\zeta}{r^2} - (\nu-1)\,\zeta\frac{u}{r^3} - \nu\zeta\frac{u'}{r^2} + 2\nu\zeta\frac{u}{r^3}\right] \tag{2.15}$$

which can also be expressed as

$$\frac{\partial H}{\partial u} = -\frac{\zeta}{(1+u')}\left[\frac{1-\nu u'}{r^2} + \frac{(1+\nu)u}{r^3}\right] \tag{2.16}$$

noting that $\zeta > 0$. Because $\nu \in [.45, .5)$ and $|u'(r)| < 1$ we can conclude that

$$\frac{1-\nu u'}{r^2} + \frac{(1+\nu)u}{r^3} > 0 \tag{2.17}$$

satisfying the condition that $\partial H/\partial u < 0$. Therefore by theorem 2.1 the solution to equation 2.7 (with boundary conditions 2.9 and 2.10) is unique.

2.2. *Mathematical analysis – isotropic deformation*

For examining the isotropic behavior of the annular region, we examine 2.7 for the case where the material properties are the same regardless of the direction of deformation. Hence, $\zeta = 1$ and equation 2.7 reduces to

$$u'' + \frac{u'}{r} - \frac{u}{r^2} - \frac{(1-\nu)}{2r}(u')^2 - \frac{(\nu-1)}{2r}\left(\frac{u}{r}\right)^2 - \frac{1}{2}\frac{d}{dr}(u')^2 - \frac{\nu}{2}\frac{d}{dr}\left(\frac{u}{r}\right)^2 = 0 \tag{2.18}$$

with the boundary conditions as stated in 2.9 and 2.10. Similar to our analysis in the orthotropic case, we can replace u with $-u$ and express 2.18 in the form as in 2.11 where H is now

$$H = -\frac{1}{(1+u')}\left[-\frac{1}{r}u' + \frac{1}{r^2}u + \frac{\nu-1}{2r}\left(u'\right)^2 + \frac{1-\nu}{2r^3}u^2 - \nu\left(\frac{u'u}{r^2} - \frac{u^2}{r^3}\right)\right] \quad (2.19)$$

with the boundary conditions defined in 2.9 and 2.10. Similarly, we examine the annular domain of the iris region $r \in (r_1, r_2)$ we see that the length of the domain is fairly small and hence it is safe to make the assumption that the solution u behaves in the manner such that$|u'(r)| < 1$. Furthermore, since the rest of the expression inside the brackets of the expression in 2.19 is in polynomial form then it is safe to conclude that H and its derivatives are continuous.

Next, we compute $\partial H/\partial u$ and get the following expression:

$$\frac{\partial H}{\partial u} = -\frac{1}{(1+u')}\left[\frac{1}{r^2} - (\nu-1)\frac{u}{r^3} - \nu\frac{u'}{r^2} + 2\nu\frac{u}{r^3}\right] \quad (2.20)$$

which can also be expressed as

$$\frac{\partial H}{\partial u} = -\frac{1}{(1+u')}\left[\frac{1-\nu u'}{r^2} + \frac{(1+\nu)u}{r^3}\right]. \quad (2.21)$$

Because $|u'(r)| < 1$ and $\nu \in [.45, .5)$ we can conclude that

$$\frac{1-\nu u'}{r^2} + \frac{(1+\nu)u}{r^3} > 0 \quad (2.22)$$

and the condition that $\partial H/\partial u < 0$ is satisfied. Therefore by theorem 2.1 the solution to 2.18 (with the boundary conditions expressed in 2.9 and 2.10) is unique.

3. Numerical Results and Simulation

The numerical simulation of the iris deformation for both the orthotropic and isotropic cases was done using the Finite Element Method (FEM). The simulation could be implemented via other numerical methods; however, we found that the FEM offers greater flexibility in regards to mesh generation. The FEM implementation consisted of converting equation 2.7 (equation 2.18 for the isotropic case) into a variational form; and discretizing our annular domain into 100 vertices that are uniformly spaced from the inner radius r_1 to the outer radius r_2 (r_2 is set to $6mm$ to represent the limbus boundary). Because the average pupil size at constriction is $3mm$ in diameter we initialize the inner radius to $1.5mm$ and solve

numerically for $u(r)$. As we vary the inner radius we continue to numerically solve for $u(r)$ noting the level of deformation of the iris tissue. Furthermore, due to the fact that the average pupil size at dilation is approximately $9.6mm$ diameter (or $4.8mm$ in radius), we use that as our stopping point. Each time we solve for $u(r)$ we compare that to the linear assumption. To visualize the deformation, we add concentric circles within our annular region that are evenly spaced from the inner to the outer radius. Once we numerically solve for $u(r)$, we move the ring located at radius r to the final position $u(r) + r$. We do the same thing for the linear assumption to see the distinction in effects.

We adopt Pamploma's metrics [15] as follows: the distance from the interior point to the center of the annular region; the distance from the interior point to the pupil boundary; and the ratio of the distance between the tracked interior point to the pupil border and the local width of the iridal disk (otherwise known as the invariance). Doing so enables us to further analyze the nonlinear effects of the interior points of the annular region for both the orthotropic and isotropic cases.

3.1. *Numerical results – orthotropic deformation*

For the numerical simulation of the orthotropic deformation, we adopt Lei et. al's [9] formulation and assumptions for determining the material parameters E_r and E_θ in order to compute ζ for the various degrees of dilation. Because it is found that the Poisson ratio for the iris $\nu \in [.45, .5)$, we chose $\nu = .49$ for our simulation. Figures 1-3 show the results for each simulation where the inner radius was changed to $2mm$, $3mm$, and $4mm$ that depict the various levels of iris deformation.

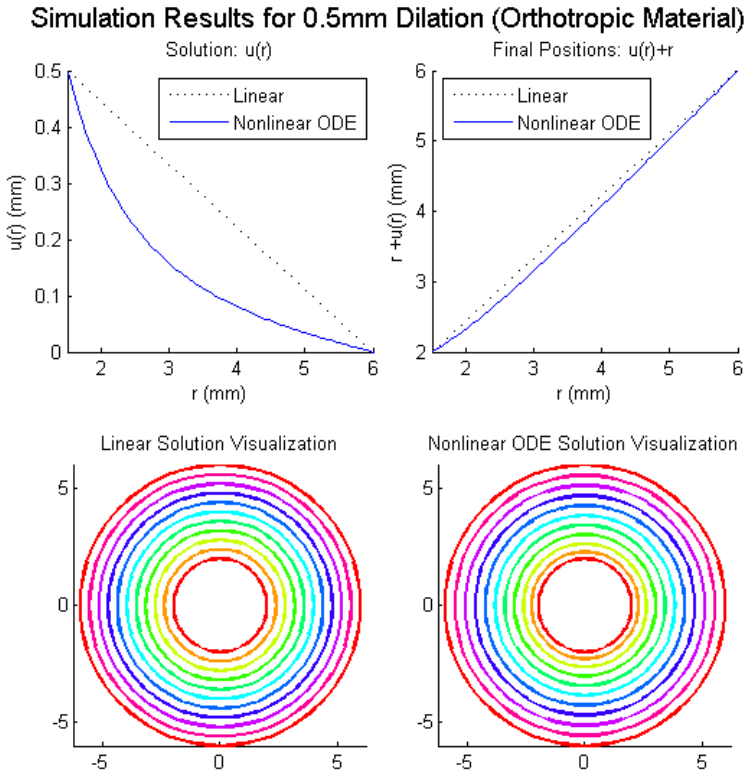

Fig. 1. Results in simulating a pupil with orthotropic material properties dilating from 1.5mm to 2.0mm. Top-left: Nonlinear solution u(r) in comparison to linear assumption. With small deformations, the difference in deformation between the two solutions relative to the size of the iris does not appear significant. Top-right: Final Bottom: Visualizations of iris given linear and ODE solutions.

In Figure 1 top left, we see the solution $u(r)$ to equation 2.7 with the pupil radius expanded to $2mm$ making the comparison to the previously assumed linear solution. We see that the solution to our boundary value problem is nonlinear as well as it appears that the tissue is compressed in the inner most regions of the iris, which is where most of the deformation occurs. Furthermore, in the top right of figure 1, we see the final positions of each point in the iris $(r + u(r))$, and find that since $u(r)$ is very small relative to the width of the iris, the difference between the two methods is small. At the bottom, we see visualizations of the iris after deformation. Initially, each concentric ring is spaced apart uniformly. We then move each ring at radius

r to $r + u(r)$ for both the linear and nonlinear solutions. Again, we find that the difference between the two methods is minimal.

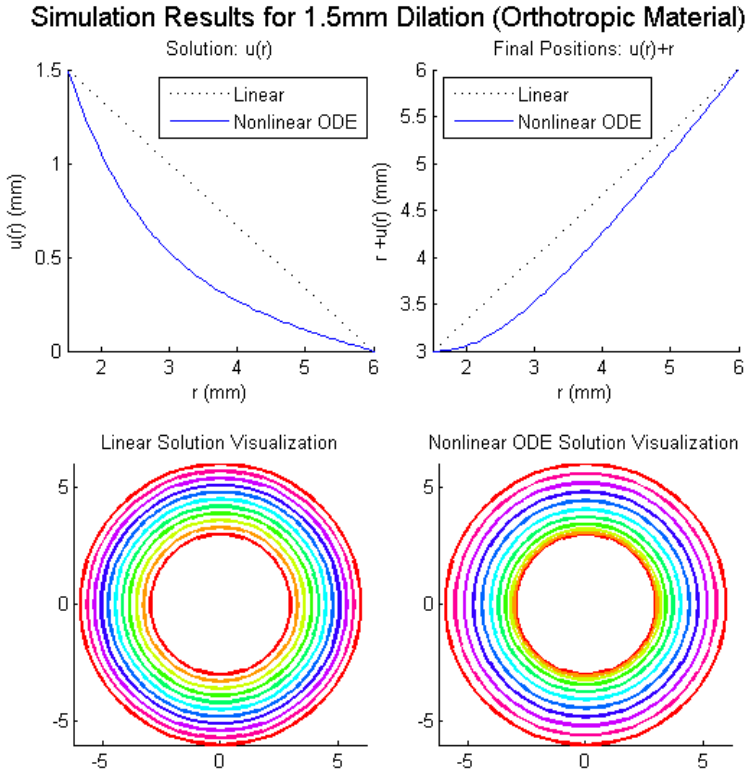

Fig. 2. Results in simulating a pupil with orthotropic material properties dilating from 1.5mm to 3.0mm. In the top-left, we see that with larger dilations, $u(r)$ continues to remain very nonlinear. Additionally, in the top-right, the differences between the nonlinear and linear solutions become significant.

In Figure 2, we see the results after simulating the pupil radius expanded to $3mm$. Again, in the top left, we see that our computed solution $u(r)$ is still highly nonlinear. However, at the top right, we now find that the differences between the linear and nonlinear solutions are much more significant relative to the width of the iris. At the bottom, in the visualizations of the iris, we can start to clearly see how the nonlinear solution deformation of the iris tissue.

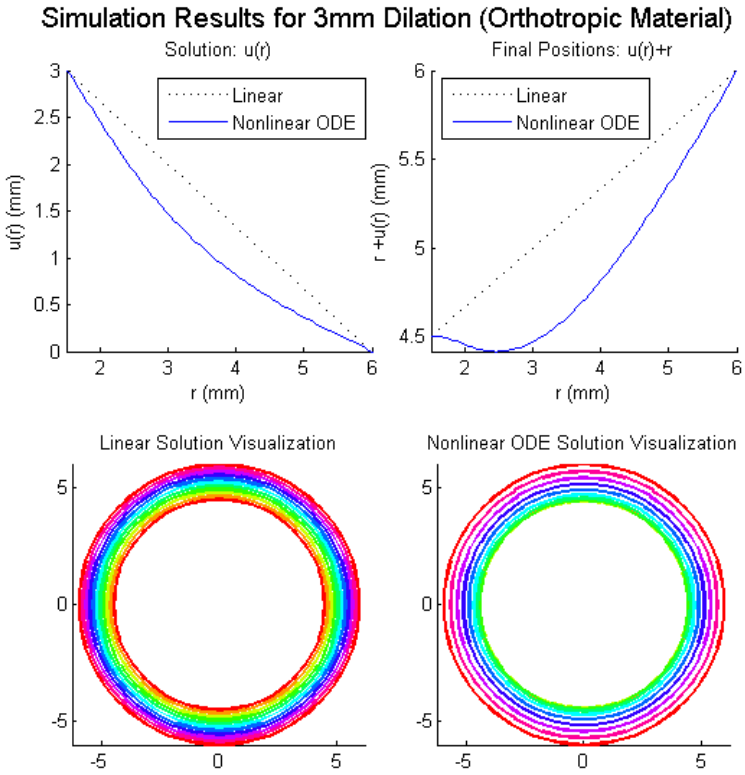

Fig. 3. Results in simulating a pupil with orthotropic material properties dilating from 1.5mm to 4.5mm. Note in the top right, the iris tissue moves backward, behind the pupil border, suggesting the need for higher-dimension simulations.

In Figure 3 we see the results after the pupil expands to 4.5mm. Here, the simulation is starting to show that the iris tissue is folding backward, which is not realistic behavior. In the top right, we see that the while the iris boundary is now at $r = 4.5mm$, elements originally at $2.5mm$ move to about $4.4mm$, behind the boundary. The visualizations at the bottom of the figure demonstrate similar results. We believe that the reason for this behavior is that this is analagous to simulating folds in the iris tissue. The reason for the effects in the radial direction is that we make the assumption that the dynamics in the z-direction are negligible.

We then ran the simulation for many more degrees of dilation and tracked several locations on the iris through time, and plotted them in figure 4. Each line in this figure represents a single point on the iris that moves as the pupil dilates. The horizontal axis represents the diameter of the pupil, and the vertical axis represents

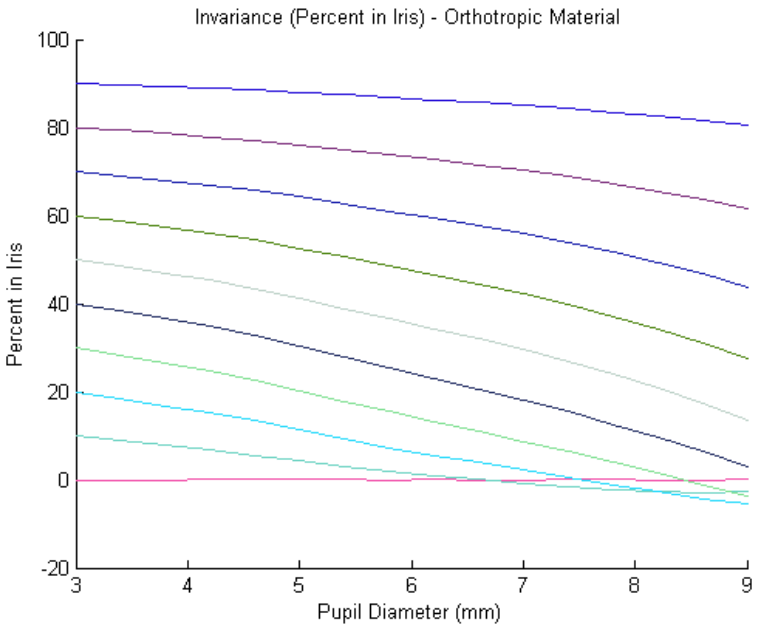

Fig. 4. Plot showing how the points interior to the iris move as the pupil dilates, given orthotropic material properties.

the percentage into the iris a given point lies. So, for example, we see that a point that was originally 10% in the iris steadily moves inward as the pupil dilates, again suggesting that the inner regions are becoming compressed. In contrast, the point originally 90% into the iris barely moves at all as the pupil dilates, generating a straight line.

3.2. *Numerical results – isotropic deformation*

Our approach to simulate the isotropic deformation was the same as that for the orthotropic case except that we set $\zeta = 1$ to account for the material parameters. The Poisson ratio ν was chosen to be .49 for our simulations for the same reasons as that of the orthotropic case. Similar to the orthotropic case, figures 5-7 show the results for each simulation where the inner radius was changed to $2mm$, $3mm$, and $4mm$ that depict the various levels of deformation in the annular region.

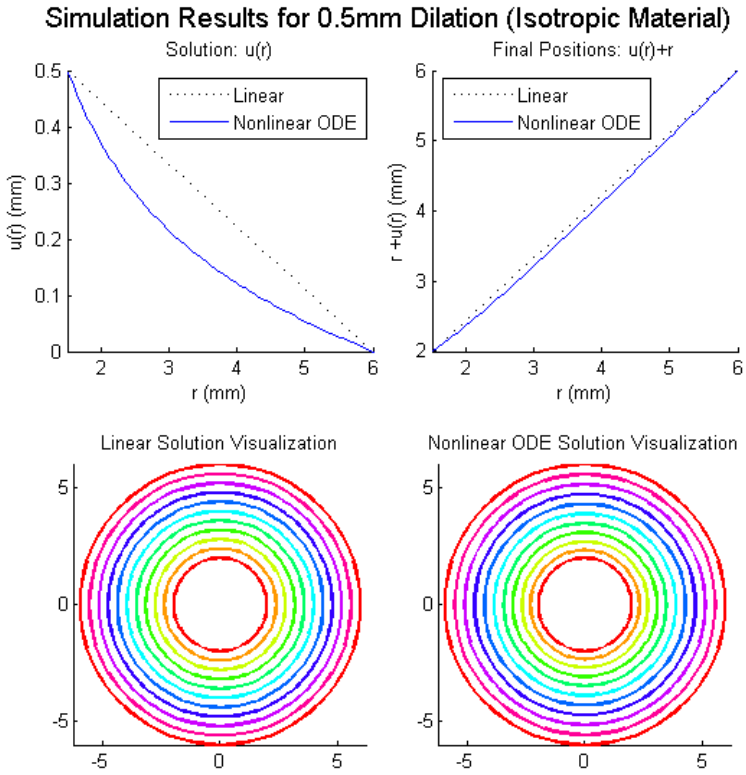

Fig. 5. Results in simulating a pupil with isotropic material properties dilating from 1.5mm to 2mm.

Analogous to the orthotropic case figure 5 shows that under small dilation the solution is very nonlinear. However, the deformation in the iris is not large enough for the difference to be significant. Compared to the orthotropic simulation, $u(r)$ does not appear to fall as rapidly at the beginning, and so we would expect the iris tissue to be slightly less compressed in the inner regions.

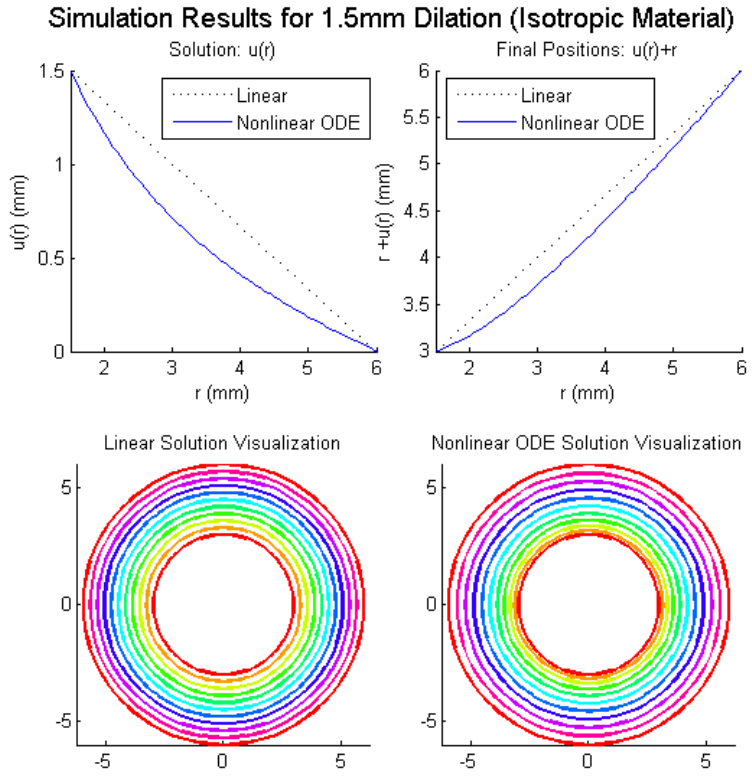

Fig. 6. Results in simulating a pupil with isotropic material properties dilating from 1.5mm to 3mm.

We reach similar conclusions for the medium deformation case in figure 6. Here, again, we see that the nonlinear deformation is starting to be significantly different than the linear deformation. Also, as in figure 5, we find that visually there is not much difference between using orthotropic material properties and isotropic material properties.

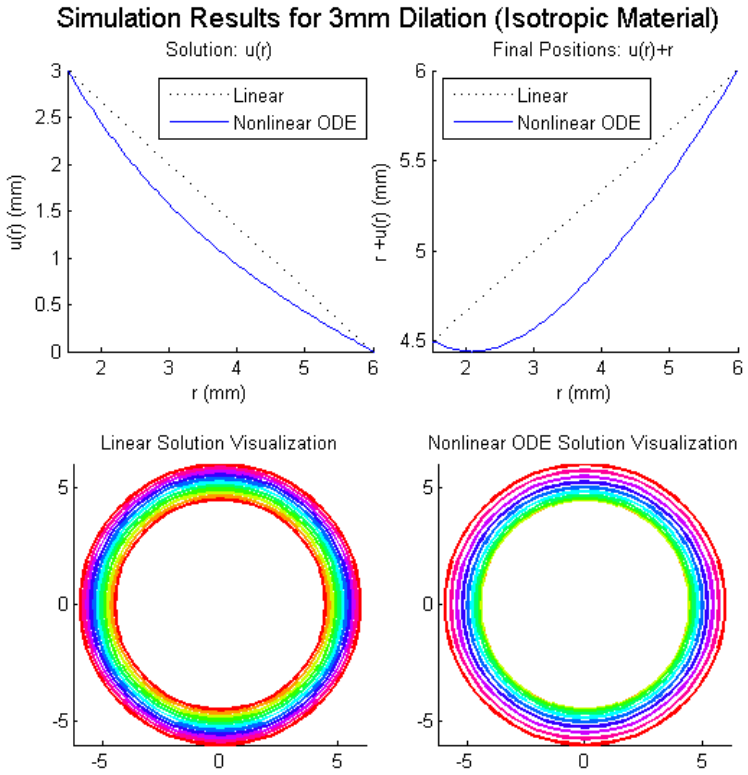

Fig. 7. Results in simulating a pupil with isotropic material properties dilating from 1.5mm to 4.5mm.

Finally, in Figure 7, we again see that the high degree of dilation is causing the simulation to produce unrealistic folding results. Interestingly, the folding does not appear to be quite as severe in the isotropic case, as we see that $r + u(r) < 4.5$ when $1.5 < r < 2.5$, whereas in the the orthotropic case, $r + u(r) < 4.5$ when $1.5 < r < 3.2$. Just as in the orthotropic case, the reason for these effects is that we make the assumption that the dynamics in the z-direction are negligible.

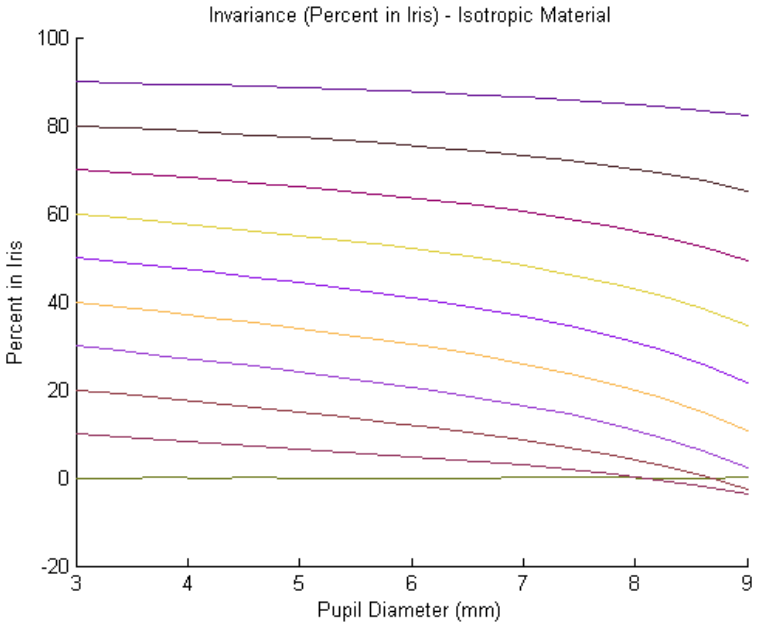

Fig. 8. Plot showing how the points interior to the iris move as the pupil dilates, given isotropic material properties.

We then again perform an analysis to track interior points of the iris as the pupil dilates, as shown in Figure 8. The results are similar to the orthotropic case, but we note that the slopes of the lines tend to be lower in this simulation. In particular, we see that the start of folding appears much later, when the pupil diameter is between $7.5 - 8mm$, as compared to the folding beginning between $6 - 6.5mm$ in the orthotropic case.

4. Conclusion and Future Work

References

1. W.F. Carroll. "A Primer for Finite Elements in Elastic Structures." John Wiley & Sons, Inc, Canada. 1999.
2. J. Daugman, "High confidence visual recognition of persons by a test of statistical independence," IEEE Transactions on Pattern Analysis and Machine Intelligence. 15(11). 1148-1161. 1993.
3. C.J. Ellis, "The Pupillary Light Reflex in Normal Subjects", British Journal of Opthamology, Vol. 65, No. 11, pp. 754-759, 1981
4. Y.C. Fung. "A First Course in Continuum Mechanics." Prentice Hall, Englewood Cliffs, NJ. 1994.

5. Y.C. Fung. "Biomechanics: Mechanical Properties of Living Tissues." Springer, NY. 1997.
6. D. Henwood and J. Bonet, "Finite Elements: A Gentle Introduction", 1996.
7. K. Hollingsworth, K. W. Bowyer, P. J. Flynn, "Pupil dilation degrades iris biometric performance," Computer Vision and Image Understanding. 113(1). 150-157. 2009.
8. A. K. Jain, P. J. Flynn and A. Ross (Editors), "Handbook of Biometrics", Springer Publishers, 2007.
9. Y. Lei et. al. "Experimental research on the mechanical properties of porcine iris." Clinical Biomechanics 23. 83-87. 2008.
10. N. Link and L. Stark, "Latency of the pupillary response", IEEE Trans. Bio. Eng., Vol. 35, No. 3, pp. 214-218, 1988.
11. A. Longtin and J.G. Milton, "Modelling Autonomous Oscillations in the Human Pupil Light Reflex Using Nonlinear Delay-Differential Equations", Bulletin of Mathematical Biology, Vol. 51, No. 5, pp. 605-624, 1989.
12. L. Ma et. al. "Efficient iris recognition by characterizing key local variations," IEEE Transactions on Image Processing. 739-750. 2004.
13. P. Moon and D. Spencer, "On the Stiles-Crawford Effect", J. Opt. Soc. Am., Vol. 34, pp. 319-329, 1944
14. A. Palazotto. "Nonlinear Analysis of Shell Structures." AIAA Education Services. 1992.
15. V. Pamploma. "Photorealistic Models for Pupil Light Reflex and Iridal Pattern Deformation." Master's Thesis, Federal University of Rio Grande do Sul, Rio Grande do Sul, Brazil. 2008.
16. H. Protter and H.F. Weinberger, "Maximum Principles in Differential Equations", Springer-Verlag, New York, 1984
17. J.N. Reddy. "An Introduction to Nonlinear Finite Element Analysis." Oxford University Press, New York. 2004.
18. H. Rohen, "Der Bau der Regenbogenhaut beim Menschen und einigen Säugern", Gegenbaur Morphology Journal, Vol. 91, pp. 140-181
19. A. Ross, "Iris Recognition: The Path Forward," IEEE Computer, pp. 30 - 35, February 2010.
20. L. Stark, "The pupil as a Paradigm for Neurological Control Systems", IEEE Trans. Biomed. Eng., Vol. 31, pp. 1925-1939
21. J. Thornton, M. Savvides, and B.V.K. Vijaya Kumar, "A Bayesian Approach to Deformed Pattern Matching of Iris Images", IEEE Transactions on Pattern Analysis and Machine Intelligence. 29(4). 596-606. 2007.
22. S. Usui and L. Stark, "A model for nonlinear stochastic behavior of the pupil", Biological Cybernetics, Vol. 45, No. 1, pp. 13-21, 1982
23. Z. Wei, T. Tan, and Z. Sun, "Nonlinear Iris Deformation Correction based on Gaussian Model." Advances in Biometrics, Lecture Notes in Computer Science, Springer Berlin/Heidelberg. 4642. 780-789. 2007.
24. H.J. Wyatt, "A 'minimum-wear-and-tear' meshwork for the iris." Vision Research. 40(2000). 2167-2176. 2000.